Mode Coupling Structure in Tokamaks

G. Lisitano

IPP III/123 September 1987

MAX-PLANCK-INSTITUT FÜR PLASMAPHYSIK

8046 GARCHING BEI MÜNCHEN

MAX-PLANCK-INSTITUT FÜR PLASMAPHYSIK

GARCHING BEI MÜNCHEN

Mode Coupling Structure in Tokamaks

G. Lisitano

IPP III/123 September 1987

Die nachstehende Arbeit wurde im Rahmen des Vertrages zwischen dem Max-Planck-Institut für Plasmaphysik und der Europäischen Atomgemeinschaft über die Zusammenarbeit auf dem Gebiete der Plasmaphysik durchgeführt.

Mode Coupling Structure in Tokamaks

G. Lisitano

Max-Planck-Institut für Plasmaphysik,

EURATOM Association

D-8046 Garching, Federal Republic of Germany

Abstract

A m=1, helically displaced current channel was identified in the ASDEX plasma interior during m=2 mode activity. This was achieved by means of simultaneous data obtained from a new gradient sensitive schlieren diagnostic and $\dot{B}_p$ measurements. They clearly show a rotational-transform-dependent coupling mechanism between the driver m=1 current helix and the m=2 perturbation of the bulk current surrounding it. The mechanism is of central importance for the development of the instability and for the theoretical understanding of mode coupling, mode locking and other varieties of mode structures in plasma.

Mode coupling processes between m=2/n=1 and m=1/n=1 magnetic islands are thought to play a dominant role in the development of current disruptions /1, 2/. The magnetic-island structures are predicted by the theory to develop at q=m rational surfaces centred on the magnetic axis /3/. Experimentally, the islands are, however, only indirectly inferred from the poloidal phase distribution of magnetic pick-up coil oscillations /4/. In particular, since the $\dot{B}_p$ oscillations are induced by the perturbed external poloidal field, they are not adequate to determine the radial distribution of the current perturbation. Recent attempts to investigate the perturbation in the plasma interior make use of tomographic imaging /5, 6/ of fluctuating soft-X-ray (SX) emission /7/. Despite intense work in this domain, line integrals and the unresolved dependence of SX on particle density, temperature and impurity components have, however, so far prevented a coherent picture of mode structures in plasma from being obtained.

Owing to its high sensitivity to variations of the density gradient, a new schlieren diagnostic /8/ exhibits fairly good spatial resolution. Applied to a representative cycle of an almost steady-state m=2, n=1 current perturbation in ASDEX, the schlieren measurements reported in this report localize an m=1 helical displacement of a highly constrained central density peak. By comparing the fast-time resolved contour of the poloidally projected plasma displacement with that of the perturbed external Bp field, the schlieren study provides important new information about magnetohydrodynamic (MHD) mode activity in plasma. These results clearly show a rotational-transform-dependent coupling mechanism between the driver m=1 helical displacement of the current peak and an m=2 perturbation of the bulk current surrounding it. Besides clarifying several hitherto unresolved features of current disruptions, the observed helical current displacement

in the plasma interior has fundamentally new implications for the theoretical understanding of the large variety of mode structures in plasma.

Figure 1 shows the schlieren signals provided by five λ=2 mm pencil beams exploring the poloidal plane at a distance Δ=0 cm, ±10 cm and ±20 cm from the midplane of the tokamak. The two hump wave forms on chords ±10 cm clearly indicate the four passages of a steep density gradient during one perturbation cycle. The individual gradients measured by each schlieren beam are first used to determine the density perturbation model shown in Fig. 2(a). The model represents the poloidal projection of a helically displaced steep peak in the plasma interior. In a numerical simulation experiment where all experimental facilities pertaining to the schlieren diagnostic are simulated as in real space, this model uniquely reproduces, as shown in Fig. 2(b), the actual schlieren wave forms of representative cycles 1, 5 and 6 of Fig. 1. (Details in Lisitano /8/.)
The signals were recorded during an L-phase of deuterium injection into deuterium plasma dominated by the m>1, n=1 mode /9/. The injection power, plasma current, particle density and safety factor are NI = 4 MW, Ip = 0.32 MA, n_e=3x10^{13} cm^{-3} and q(a) = 3.3, $q(a) = 2\pi a^2 B_T/\mu_o R I_p$. As indicated by the violent decay of β and n_e on transition to the L-phase (details in Klüber /9/), the steep peak in the central region of the plasma, see Fig. 2(a), is probably produced by resistive current constriction from the cold gas surrounding the plasma. Under these discharge conditions, the onset of the m=1 driver perturbation of the current peak may then originate from resistive excitation of JxB forces on it.

As the density perturbation model of Fig. 2(a) is well correlated with $\dot{B}_p$ fluctuations, the model should also apply to the current perturbations that generate the external inductor field. Assuming therefore identical current and density distributions, the B_p field perturbation contour delivered by the schlieren measurements in the plasma interior is compared in the following with that of the external B_p field perturbation derived from the simultaneously detected Mirnov oscillations. The latter are shown in Fig. 3 in accordance with the poloidal angle θ at which they were detected. The first trace of Fig. 3 also shows the schlieren signals of the chord Δ = +10 cm of Fig. 1. The schlieren signals establish the period T of a complete poloidal excursion of the displaced plasma centre. The poloidal phase distribution of the Mirnov oscillations at a given instant is shown in Fig. 3, left. The total poloidal phase variation of 4π clearly identifies the m=2 mode number of the oscillations. Such an m=2 mode is also identified in Fig. 3 by the two travelling waves B and C, obtained by joining points of equal phase /10/.

A straight-line approximation of the travelling-wave path of Fig. 3 allows straightforward calculation /10/ of the poloidal B_p field distribution $B_p = B_{max} \cos m(\theta+\pi/2)$, which induces the Mirnov oscillations $e(\theta) = vB_p(\theta) = (\omega/m) r B_{max} \cos\left[\omega t - m(\theta+\pi/2)\right]$ at the r = const. radial position of the coils. In the above expression, the time t=0 corresponds to the passage of the plasma centre through the midplane, at $\theta = 0^o$, as indicated by dashed lines in Fig. 3. With equal amplitude of the Mirnov oscillations being assumed, the poloidal field exhibits the m=2 variations indicated in Fig. 4 by the last, external traces. Figure 4 also shows the angular position of the plasma centre, vector A, and that of the two travelling waves, vectors B and C, at four instants t/T = 0, 1/4, 1/2 and 3/4. Within a period T, the

two travelling waves travel a poloidal angle π at opposite angles. They therefore exhibit a reduced synchronous velocity, $\pi/T = \omega/2$, as compared with the rotation speed ω of the projected plasma centre on the poloidal plane.

For the assumed identical current and density distributions, the perturbation model of Fig. 2(a) gives the radial profile of the B_p field perpendicular to the machine midplane. On the basis of this field profile and of the position of the plasma centre, the poloidal contour of the B_p field perturbation in the plasma interior is extended, as shown in Fig. 4, to that of the measured B_p field external to the plasma. To provide a clear representation in Fig. 4, the m=2 ellipticity of the perturbed external B_p field contour has been exaggerated. Considering that $\tilde{B}_p/B_p$ is only a few per cent, the dominant feature in Fig. 4 is the projected m=1 helical displacement of the current channel. As the m=2 B_p field perturbation only represents a very slight modulation of the bulk current surrounding the highly contrained current helix, the B_p field contours of Fig. 4 call for a sequence of flux-conserving equilibria typical of Shafranov pressure effects /11/.

From Fig. 4 it is clearly seen that the instability mechanism depends on the formation of a steep current channel in the plasma interior. At low q ($q<1$) this current channel is subjected to the observed m=1 helical displacement, which excites the $m>1$ perturbations of the bulk current surrounding it. The driver m=1 current helix and the $m>1$ satellite perturbations of the bulk current are coupled to each other by the local B_T/B_p field rotational transform. This is clearly seen in Fig. 4 from the m=1 and m=2 rotational transform phase-relation and in Fig. 3, left, from the instantaneous phase distribution of the Mirnov oscillations. Assuming for

the latter a constant B_p field along the minor radius r, at which B_p rotates, the observed phase distribution $\psi(\theta)=k_\theta\theta$ closely follows the dependence of the B_T field on the r/R toroidicity given by the angular wave number $k_\theta=m(\theta)$ of the perturbation: $k_\theta=m\left[1+(r/R)\cos\theta\right]^{-1}$.

The perturbation model of Fig. 2(a) represents a powerful redistribution mechanism for the incoming additional heating power to the tokamak plasma. Since line-integral measurements are very sensitive to the global spatial redistribution of the incoming energy, they reproduce sawtoothing events well. They are, however, rather insensitive to the detailed redistribution fluctuations of the various plasma components in the plasma interior. It should therefore not be surprising if for some discharge conditions the heat energy redistribution is such that sawteeth without precursors are seen on SX line-integrated signals /12/.
This particular case is met in ASDEX during sawtoothing in some additionally heated low-q, low-density discharges, where, except for a single non-central exploring chord, all other schlieren and line-integrated measurements of the λ=2 mm phase shift may not exhibit coherent precursor fluctuations on sawteeth. As the displacement radius of the current helix is small, the magnetic pick-up coils do not detect oscillations during such sawteeth either.

These observations can be compared with various theoretical models. A common property of these models is the assumption of a centred radial current distribution /3/. As the current is increased in time, one theory predicts symmetric m=2 magnetic islands moving towards the limiter /1/. In other theories, coupling and non linear interaction between various mode structures is invoked to explain current disruptions /2/. For internal

disruptions in sawtoothing plasma, the Kadomtsev model /13/ predicts magnetic island formation by magnetic flux reconnection inside and outside the q=1 surface. This description is not consistent with the experimental observations made with schlieren and $\dot{B}_p$. Contrary to the theoretical predictions of radially displaced magnetic islands growing around on initially unperturbed plasma centre, these observations show the opposite, i.e., a growing helical displacement of the plasma centre. This experimentally observed mechanism has fundamentally new implications for clarifying various hitherto unresolved MHD features.

Without any claim to detailed theoretical treatment, such implications are briefly outlined for the following few examples of MHD events.

Mode locking: Two mode-locking events are shown in Fig. 1, first trace, by the relaxing frequency reduction of the m=2 Mirnov oscillations. Contrary to theoretical predictions /14/, both the frequency and the amplitude reduction in Fig. 1 can be explained by a rapid enlargement of the m=1 current helix within a few perturbation cycles. Such poloidal enlargement of the helix has, in fact, a counteracting, slowing-down effect on the poloidal rotation of the projected m=1 current centre.

As is indicated by H_α pulses (not shown in Fig. 1) occurring on frequency reduction, the rapid enlargement of the helix is related to interaction of the plasma edge with cold gas surrounding it. When the plasma edge interaction is somewhat larger, at t=1.235 s in Fig. 1, the steep current profile collapses into the originally unperturbed position, but with a flat current profile. This in turn extinguishes all mode activity.

Sawooth crash: The observed time scale of a few hundred microseconds for the sawtooth collapse in large tokamaks /12/ is very consistent with recent schlieren observations of rapid enlargement of the current peak displacement radius within a fraction of a current perturbation cycle /8/. Depending on the resistive discharge conditioning, the minor helix radius increases to a threshold value where collapse of the internal current helix is indirectly excited at large plasma radii by the resistive interaction of the m>1 perturbed bulk plasma with cold gas surrounding it. The spiralling collapse of the current peak is quite similar to the collapse phase of mode locking but further experimental investigations are required to confirm details of this mechanism.

In conclusion, as compared with the relatively flat line-integrated display, the new gradient-sensitive measurements provide a high-relief display of mode structure in plasma. Contrary to theoretical prediction of magnetic islands on q=m rational magnetic surfaces, the schlieren measurements clearly show a dominant m=1 helical displacement of a current channel in the plasma interior. The current displacement provides m>1 perturbations of the bulk current surrounding it. The various perturbations are inherently coupled to each other by the local rotational transform value imposed by the rotating poloidal field. This clearly demonstrates that the observed m=2 mode activity preceding current distribution represents a severe radial displacement of the helically perturbed plasma centre.

The author is indebted to the ASDEX team for their experimental support of this work.

References

/1/ A. Sykes and J.A. Wesson, Phys. Rev. Lett. 44, 1215 (1980).

/2/ S. Tsuji, Y. Nagayama, and K. Miyamoto, Nucl. Fus. 25, 305 (1985).

/3/ A.H. Glasser, H.P. Furth, and P.H. Rutherford, Phys. Rev. Lett. 38, 234 (1977).

/4/ S.V. Mirnov and I.B. Semenov, Sov. At. Energy 30, 22 (1971).

/5/ R.S. Granetz and J.F. Camacho, Nucl. Fus. 25, 727 (1985).

/6/ M.A. Dubois, D.A. Marty, and A. Pochelon, Nucl. Fus. 20, 1355 (1980).

/7/ S. von Goeler, W. Stodiek, and N. Sauthoff, Phys. Rev. Lett. 33, 1201 (1974).

/8/ G. Lisitano, Rev. Sci. Instrum. 58, 249 (1987); G. Lisitano, in Proceedings of the 14th European Conference on Controlled Fusion and Plasma Physics, Madrid, Spain, 1987 (unpublished) Vol. III, p. 1334.

/9/ O. Klüber et al., in Proceedings of the 13th European Conference on Controlled Fusion and Plasma Physics, Schliersee, Germany, 1986 (unpublished) Vol. I, p. 136.

/10/ E. Levi, Electromechanical Power Conversion (McGraw-Hill, New York, 1966), pp. 226-231.

/11/ R.A. Dory and Y.-K.M. Peng, Nucl. Fus., 17, 21 (1977).

/12/ A.W. Edwards et al., Phys.Rev.Lett. 57, 210 (1986).

/13/ B.B. Kadomtsev, Fiz. Plazmy 1, 710 (1975) [Sov. J. Plasma Pys. 1, 389 (1975)].

/14/ M.F.F. Nave and J.A. Wesson, in Proceedings of the 14th European Conference on Controlled Fusion and Plasma Physics, Madrid, Spain, 1987 (unpublished) Vol. III, p. 1103.

Figure Captions

Fig. 1: Characteristic two-hump schlieren wave forms at $\Delta = \pm 10$ cm, indicating an m=1-like density distribution structure in the plasma interior. The last trace shows the simultaneously detected fluctuations of the line-integrated density signals.

Fig. 2: (a) Radial density profile and schlieren perturbation model used to obtain the simulated signals of (b). (b) Numerical simulation of cycles 1, 5 and 6 of the actual schlieren signals of Fig. 1.

Fig. 3: Schlieren signals, first trace, and simultaneously detected Mirnov oscillations.

Fig. 4: B_p field contour and angular position of the plasma centre, vector A, and of the two travelling waves of Fig. 3, vectors B and C, at four instants t/T = 0, 1/4, 1/2 and 3/4. The dotted circles indicate the r=const. position of the Mirnov coils.

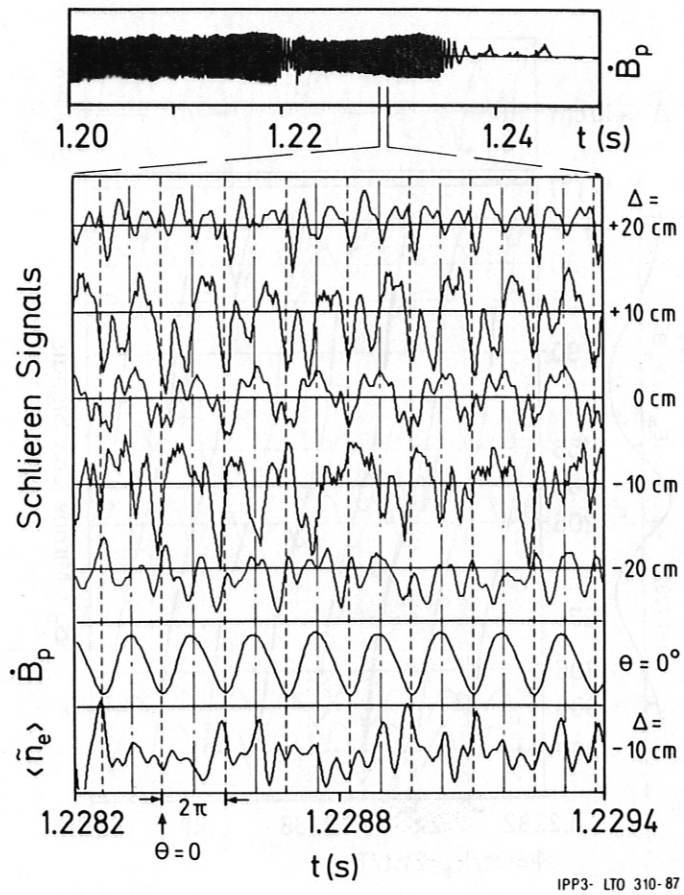
$\dot{B}_p$
1.20
1.22
1.24
t (s)
Schlieren Signals
Δ = +20 cm
+10 cm
0 cm
-10 cm
-20 cm
$\dot{B}_p$
θ = 0°
$\langle \tilde{n}_e \rangle$
Δ = -10 cm
2π
1.2282
θ = 0
1.2288
1.2294
t (s)
IPP3- LTO 310-87

Fig. 1

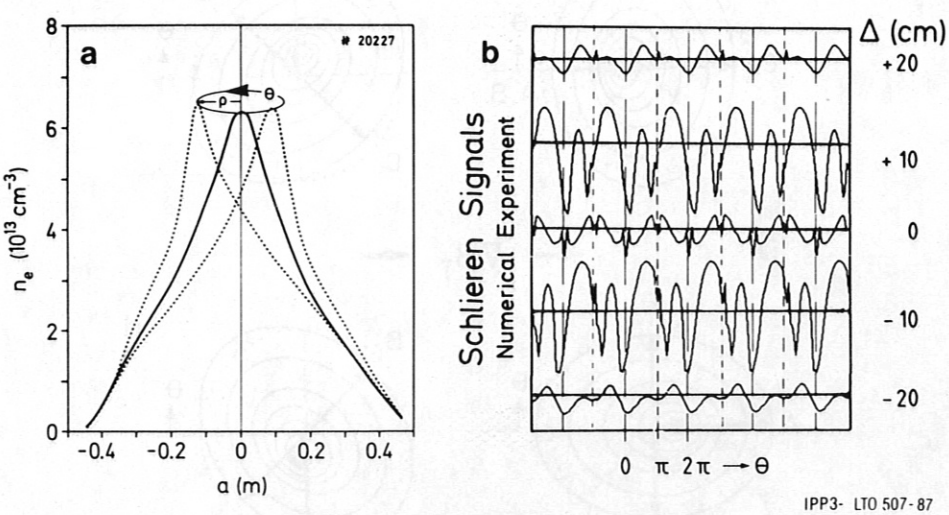
a
20227
ρ
θ
n_e (10^{13} cm^{-3})
8
6
4
2
0
-0.4
-0.2
0
0.2
0.4
a (m)
b
Schlieren Signals
Numerical Experiment
Δ (cm)
+20
+10
0
-10
-20
0
π
2π
→ θ
IPP3- LTO 507-87

Fig. 2

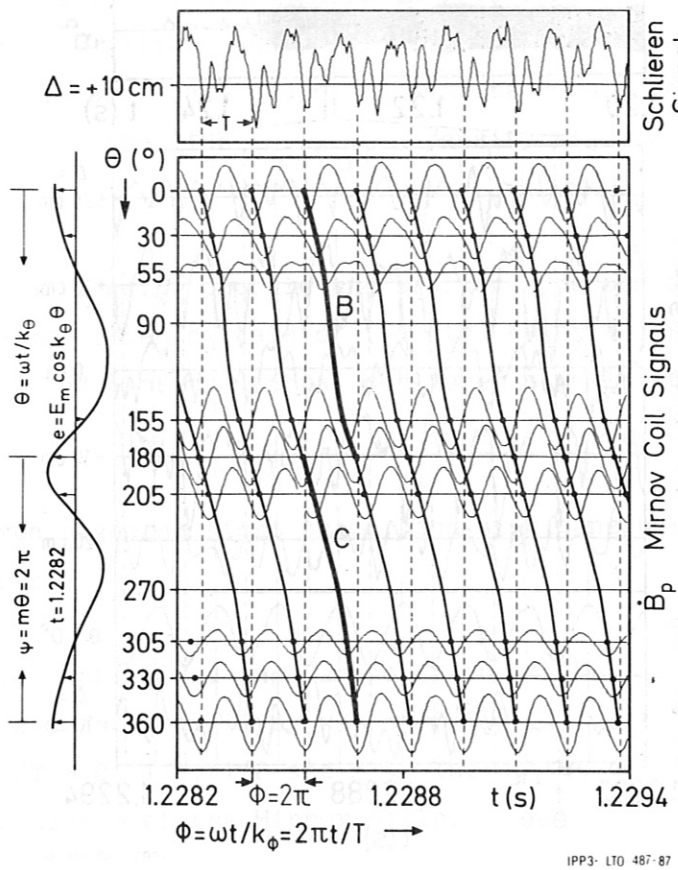
Δ = +10 cm
T
Schlieren Signal
Θ (°)
0
30
55
90
155
180
205
270
305
330
360
B
C
Θ = ωt/k_Θ
e = E_m cos k_Θ Θ
ψ = mΘ = 2π
t = 1.2282
Ḃ_p Mirnov Coil Signals
1.2282
Φ = 2π
1.2288
t (s)
1.2294
Φ = ωt/k_Φ = 2πt/T
IPP3- LTO 487-87

Fig. 3

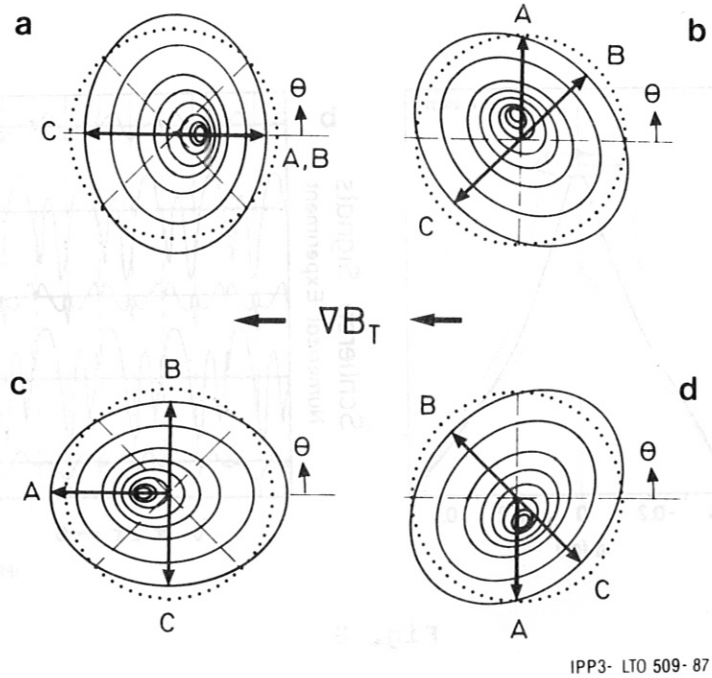
a
b
c
d
A
B
C
Θ
A,B
∇B_T
IPP3- LTO 509-87

Fig. 4